

# PHYSICS OF HIGH PERFORMANCE JET PLASMAS IN D-T

The JET Team<sup>1</sup>

(Presented by M.L. Watkins)

JET Joint Undertaking,  
Abingdon, Oxfordshire,  
United Kingdom.

## Abstract

JET has recently operated with deuterium-tritium (D-T) mixtures, carried out an ITER physics campaign in hydrogen, deuterium, D-T and tritium, installed the Mark IIGB “Gas Box” divertor fully by remote handling and started physics experiments with this more closed divertor. The D-T experiments set records for fusion power (16.1 MW), ratio of fusion power to plasma input power (0.62, and  $0.95 \pm 0.17$  if a similar plasma could be obtained in steady-state) and fusion duration (4 MW for 4 s). A large scale tritium supply and processing plant, the first of its kind, allowed the repeated use of the 20 g tritium on site to supply 99.3 g of tritium to the machine. The H-mode threshold power is significantly lower in D-T, but the global energy confinement time is practically unchanged (no isotope effect). Dimensionless scaling “Wind Tunnel” experiments in D-T extrapolate to ignition with ITER parameters. The scaling is close to gyroBohm, but the mass dependence is not correct. Separating the thermal plasma energy into core and pedestal contributions could resolve this discrepancy (leading to proper gyroBohm scaling for the core) and also account for confinement degradation at high density and at high radiated power. Four radio frequency heating schemes have been tested successfully in D-T, showing good agreement with calculations. Alpha particle heating has been clearly observed and is consistent with classical expectations. Internal transport barriers have been established in optimised magnetic shear discharges for the first time in D-T and steady-state conditions have been approached with simultaneous internal and edge transport barriers. First results with the newly installed Mark IIGB divertor show that the in/out symmetry of the divertor plasma can be modified using differential gas fuelling, that optimised shear discharges can be produced, and that krypton gas puffing is effective in restoring L-mode edge conditions and establishing an internal transport barrier in such discharges.

## 1. INTRODUCTION

Since the last IAEA Conference in Montreal in 1996 [1], the Joint European Torus (JET) has continued to address major issues in fusion physics and technology for which it is uniquely suited. In particular, JET being a one-third scale model of the International Thermonuclear Experimental Reactor (ITER) [2] and with a very similar plasma and divertor configuration, is the nearest in size and operating conditions to a Next Step tokamak reactor. Furthermore, JET has been designed from the outset for deuterium-tritium (D-T) operation and has comprehensive tritium processing and remote handling systems. Following the closure of TFTR which operated successfully with D-T from 1993 until 1997 [3], JET is now the only experiment able to operate with D-T. In the last two years, JET has: developed plasma performance and understanding sufficiently for D-T operation in 1997 (DTE1) [4-6]; carried out an ITER physics campaign in hydrogen, deuterium, D-T and tritium; installed the Mark IIGB “Gas Box” divertor fully by remote handling in the activated environment which followed DTE1; and started physics experiments with this more closed divertor.

This paper concentrates on confinement issues critical for high performance (Section 2), D-T performance and related physics (Section 3), tritium supply, plasma concentrations and in-vessel inventory (Section 4) and the first results with the Mark IIGB “Gas Box” divertor (Section 5) before the summary and conclusions in Section 6.

Three modes of high confinement in JET perform consistently better than the L(low)-mode of confinement: the ELMy H-mode, the ELM-free H-mode and the optimised magnetic shear mode (Fig. 1).

---

<sup>1</sup> See Appendix.

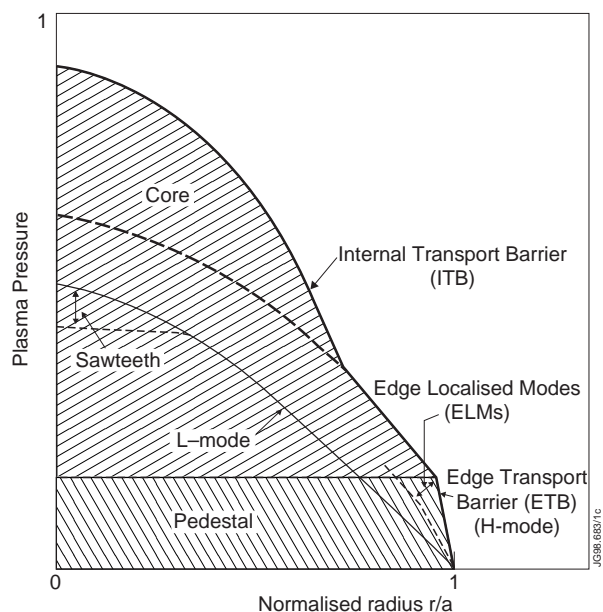


Fig.1. Characteristic plasma pressure profiles in different modes of tokamak operation: L-mode, H-mode with Edge Transport Barrier and optimised shear mode with Internal Transport Barrier.

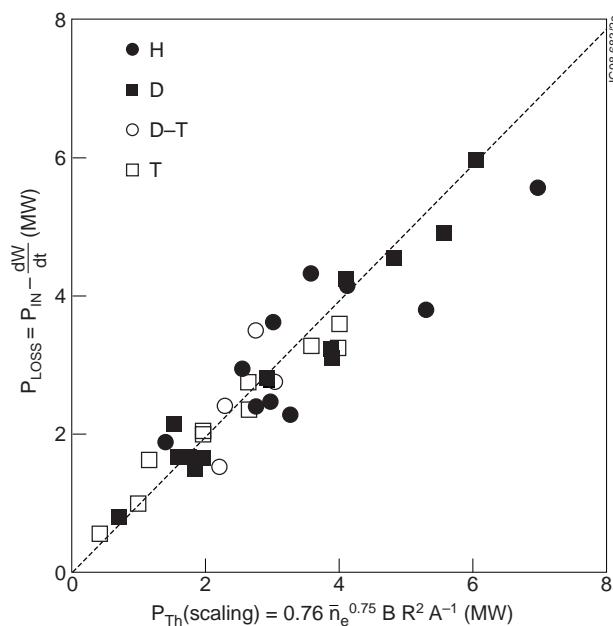


Fig. 2 Plasma loss power for ELMy H-mode discharges in hydrogen, deuterium, deuterium-tritium and tritium plotted against the ITER scaling for the H-mode threshold power modified to include an inverse mass dependence.

The ELMy H-mode benefits from the formation of an Edge Transport Barrier (ETB) which is partially eroded by regular Type I Edge Localised Modes (ELMs) which, however, also help to maintain steady plasma conditions. This is the only steady-state regime which has been experimentally validated, and is the standard operating mode foreseen for ITER. Section 2 deals with the characterisation of this mode in D-T to allow more accurate assessments of the ignition margins and the heating requirements of ITER. The conditions needed for high confinement (that is, the threshold for the formation of an ETB) and the scaling of energy confinement in this regime are discussed in Sections 2.1 and 2.2 respectively, particular emphasis being placed on the dependences on isotopic mass ( $A$ ).

The global energy confinement time of these discharges is well documented empirically (the ITERH-97Py scaling [7]), also in terms of the relevant dimensionless parameters (Section 2.3), and can be used with confidence for extrapolation to ITER. However, the mass dependence of the ITERH-97Py scaling conflicts with its otherwise close to gyroBohm scaling. This might be explained by separating the thermal energy of the plasma into contributions from the core and pedestal (Fig. 1, Section 2.4 and [8]). Of particular importance is the scale length of the ETB since this affects the pedestal energy. The scaling of the core energy is also important since this determines the capacity for high fusion performance.

Confinement is known to fall below the ITERH-97Py scaling at the high density and radiated power conditions foreseen for ITER, and this may be related to a fall in the pedestal energy. Furthermore, neoclassical tearing modes are thought to be responsible for a  $\beta$  limit in long pulse discharges which is well below the limit set by ideal MHD instabilities. These issues are addressed in Sections 2.5 [9] and 2.6 [10], respectively. Local transport analysis of ELMy H-modes, hot ion ELM-free H-modes and optimised shear modes confirms that the transport in the edge and core are different and this is discussed in Section 2.7.

The hot ion ELM-free H-mode is the traditional mode for high performance, but is limited by the onset of a giant ELM which destroys the fully developed ETB. Nevertheless, the Preliminary Tritium Experiment (PTE), using a mixture of only 11% tritium and 89% deuterium in an hot ion ELM-free H-mode, produced a peak fusion power of 1.7 MW averaging 1 MW over 2 s and a fusion gain  $P_{\text{fus}}/P_{\text{in}}=0.12$  [11]. This was the first controlled production of significant fusion power and the development of the hot ion ELM-free H-mode since that time warranted its further study in D-T during 1997 (DTE1) [12].

Performance in the optimised shear mode benefits from the formation of an Internal Transport Barrier (ITB) which has been maintained in combination with an L-mode, ELMy H-mode or ELM-free H-mode edge. This is an advanced mode of tokamak operation which uses profile control techniques to engineer high plasma confinement and to develop these conditions into steady-state. This concept, if successful, would give ignition and sustained burn at lower plasma current and toroidal field, thereby reducing the cost of a reactor. JET has been particularly suited to such studies by virtue of its combination of heating schemes and its current drive capability and the optimised shear scenario developed in JET has pressure profiles which are more peaked and D-D neutron yields which are higher than in the ELM-free H-mode [13,14].

All these high performance studies helped to define the issues addressed during 1997 when JET resumed D-T operation with a broad-based but closely focussed series of D-T experiments (DTE1) [4-6]. Records in fusion performance (Section 3.1) were set, the physics of high performance plasmas in D-T were validated, and specific issues of D-T technology for ITER and a reactor were addressed [15]. The most important physics objectives of DTE1 were: the heating of D-T plasmas using waves at the ion cyclotron resonance frequency (ICRF) (Section 3.2, [16]); the demonstration of alpha particle heating to confirm the process by which ignition and self-sustained burn would occur in a reactor (Section 3.3, [17]); the validation of the theory of Alfvénic instabilities induced by the alpha particles (birth energy of 3.5 MeV) (Section 3.4, [17]); and the first demonstration in D-T of the control of plasma profiles in the optimised shear mode of operation (Section 3.5, [18, 19]).

During DTE1, tritium was supplied, collected from the exhaust gases and processed by an industrial scale tritium processing plant (the Active Gas Handling System, (AGHS)). This worked in a closed-cycle with the tokamak, pumping the torus in continuous operation. Following DTE1, JET used its unique capability for remote installation for a major modification to the JET divertor. The Mark IIA divertor target was replaced successfully by the Mark IIGB “Gas Box” divertor using full remote handling in an activated environment. These two major features of fusion technology are discussed in [15].

The retention of tritium inside the vessel is also an issue of particular importance for ITER and this is discussed in Section 4 and in [20]. The first results from the physics experiments with the Mark IIGB divertor which started in early September are reported in Section 5 and [20].

## 2. CONFINEMENT ISSUES CRITICAL FOR HIGH PERFORMANCE

### 2.1. H-mode threshold power

During DTE1, the heating power needed to access the H-mode regime (the H-mode threshold power) was determined from discharges with D-T mixtures with up to 90% concentration of tritium for a wide range of plasma currents (1-4.5 MA) and toroidal magnetic fields (1-3.8 T). Following DTE1, similar experiments were carried out in hydrogen (as in ASDEX [21] and JFT2-M [22]). These experiments have allowed the effect of isotope mass on the H-mode threshold power to be determined, the most notable result being that, in comparison with pure deuterium, the H-mode threshold power was lower in D-T and lower still in pure tritium, scaling roughly as the inverse of the isotopic mass ( $A^{-1}$ ) of the plasma mixture. This can be seen in Fig. 2 which shows the loss power from the plasma plotted as a function of the scaling  $P_{Th}=0.76n_e^{0.75}B R^2 A^{-1}$ , which has been modified from that used for ITER [2] by the inclusion of an inverse mass dependence (the constant of proportionality has also been adjusted to give the best fit to these JET data).

These results indicate that the power needed to access the H-mode in a pure tritium plasma (for example, during the start-up phase when it is important to achieve the H-mode as early as possible) is reduced by 33%, while the H-mode threshold power for a 50:50 mixture of deuterium and tritium is reduced by 20%. This is very favourable for ITER, the operational flexibility of which would thus be increased.

### 2.2. Energy confinement in ELMy H-modes

Before, during and after DTE1, steady-state ELMy H-modes were obtained for a wide range of plasma currents (1-4.5 MA) and toroidal magnetic fields (1-3.8 T) in hydrogen, deuterium, D-T and

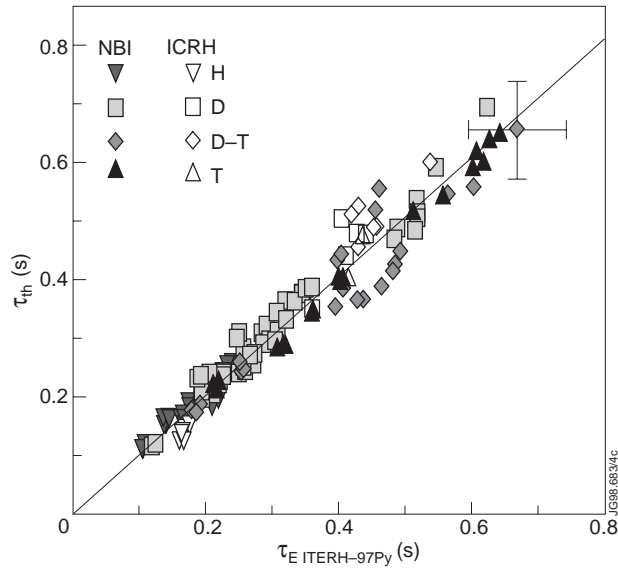


Fig. 3 Measured thermal energy confinement times in hydrogen, deuterium, deuterium-tritium and tritium ELMy H-mode discharges plotted against the ITERH-97Py scaling law.

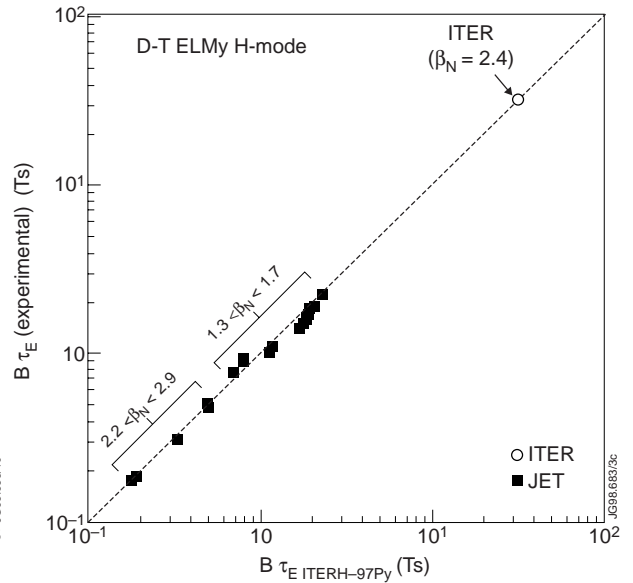


Fig. 4 Measured thermal energy confinement times of ITER similarity ELMy H-mode discharges in D-T plotted against the scaling law used in ITER projections. The operating point of an ignited ITER is also shown.

tritium. The global energy confinement times were found to be consistent with the most recent version of the multi-machine data base for this type of discharge (the ITERH-97Py scaling [7]), with its  $A^{0.2}$  isotope mass dependence providing an acceptable fit (Fig. 3). Due to the influence of mass on the H-mode threshold power and ELM behaviour, it was not possible to obtain the same density for the same input power under all operating conditions. However, a more refined data set with matched power and density in H, D, D-T and T plasmas has been constructed and this shows practically no mass dependence ( $A^{0.03 \pm 0.08}$ ). This is difficult to explain since a pure gyroBohm scaling has an  $A^{-0.2}$  mass dependence.

### 2.3. ITER demonstration pulses in D-T

ITER demonstration pulses preserve all the relevant dimensionless parameters [23] (such as the normalised plasma pressure  $\beta_N$ , collisionality  $\nu^*$  and the edge safety factor  $q_{95}$ ) close to the values of an ignited ITER, except for the normalised plasma size (the dimensionless Larmor radius,  $\rho^* = \rho_i/a$ ). On JET, the level of additional heating power prevents such demonstration pulses being produced at the highest level of performance, but at lower toroidal field and plasma current (e.g. 2 MA/2 T), the  $\beta_N$  (2.4) and collisionality of an ignited ITER have been closely matched and  $q_{95}$  was also close to the ITER value ( $q_{95}=3.2$ ). Such a JET discharge in D-T forms the basis of a series of “wind tunnel” experiments (Fig. 4) which are found to scale close to gyroBohm (except for the mass dependence) and extrapolate to ignition in ITER. In fact, a gyroBohm extrapolation from this ITER demonstration pulse gives ignition at 1.8 GW (or  $Q=5.8$  for a Bohm extrapolation) for ITER operating at 21 MA. The required density would, however, be well above the Greenwald density limit which scales as  $I/a^2$  [24].

### 2.4. Towards a theoretical basis for confinement

#### 2.4.1. Separation of confinement into core and pedestal contributions

To reach a theoretical understanding of global energy confinement, it may be useful to separate the total thermal energy of the plasma into two contributions (Figs. 5): a pedestal energy (Fig. 5(a)) which is determined from the edge temperature and density (assuming equal electron and ion temperatures at the plasma edge); and a core energy (Fig. 5(b)) which is determined by subtracting the pedestal energy from the total energy. These contributions are found to scale differently with respect to mass and other

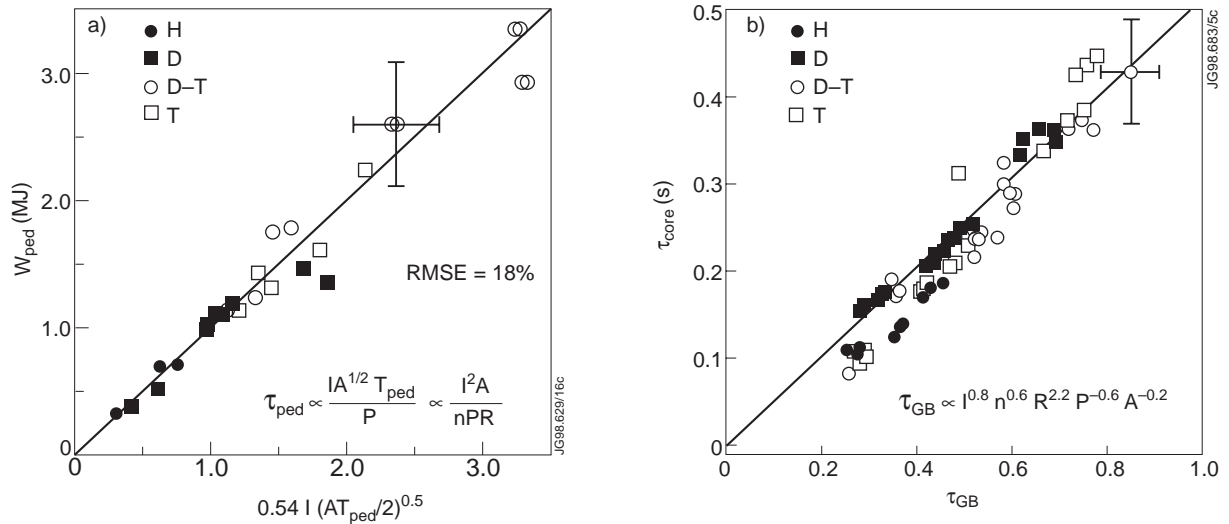


Fig. 5 (a) Pedestal energy plotted against that expected from an edge pressure gradient limited by ballooning modes over a thermal ion poloidal Larmor radius and (b) the thermal confinement time of the core plasma plotted against the best fit for the mass dependence in a pure gyroBohm scaling for ELMy H-mode discharges in hydrogen, deuterium, deuterium-tritium and tritium.

significant parameters. The scaling of the pedestal energy has been obtained from a free fit, constrained to specific physics models. A particularly good fit is to a model which assumes that the gradient of the plasma pressure in the edge is limited by ideal ballooning mode instabilities over a distance characterised by an ion Larmor radius [25]; this leads to a positive mass dependence ( $A^{0.5}$ ), as shown in Fig. 5(a). The best fit is with the Larmor radius of the thermal ions. The corresponding core energy confinement time (Fig. 5(b)) is found to be consistent with the  $A^{-0.2}$  mass dependence which would be expected from a pure gyroBohm scaling, generic of theoretical transport models based on turbulence with a scale length given by the ion Larmor radius.

An expression for the total energy confinement time may then be obtained [8] by adding the two contributions. This gives an off-set non-linear form which is similar to that derived in [26]. The core contribution, being consistent with gyroBohm scaling, would be favourable for extrapolations to a reactor; the pedestal scaling shows degradation with increasing density and radiated power, but requires the scale length for the edge transport barrier to be determined before it can be used with confidence for extrapolations to a reactor.

#### 2.4.2. Width of the edge transport barrier

There is strong evidence that the width of the edge transport barrier depends upon the poloidal ion Larmor radius [8, 9, 27]. However, depending on plasma conditions, this has been associated with thermal or fast ions. There are some indications in the JET data that the Larmor radius of fast ions produced by NB heating determines the scale length of the edge pressure gradient. For example, on-axis ICRF heating produces fewer fast ions in the edge compared with NB injection and such ICRF heated discharges are characterised by high frequency Type III ELMs and low edge pressure in comparison with NB heated discharges with the same input power. In hot ion ELM-free H-mode discharges, a mass dependence is seen, with the pedestal energy being significantly higher with tritium injection into a tritium plasma than with deuterium into deuterium. Moreover, with tritium injection into a deuterium plasma, the pedestal pressure is also high. While the Larmor radius of fast ions provides a better fit of ELMy H-mode discharges without gas fuelling, a similar analysis of gas fuelled discharges shows the opposite trend [28]. More refined experiments are currently in progress.

Irrespective of what determines the pedestal width, the loss in confinement and increase in Type I ELM frequency with gas fuelling at high density and with high radiated power can be associated with a cooling of the plasma edge and a loss of pedestal energy. This could account for the degradation of confinement under these conditions.

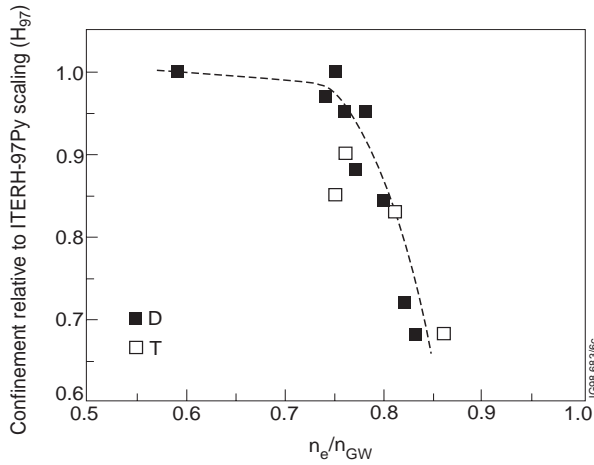


Fig. 6 Energy confinement time relative to the ITERH-97Py scaling versus density relative to the Greenwald density. Confinement starts to degrade above 75% of the Greenwald density.

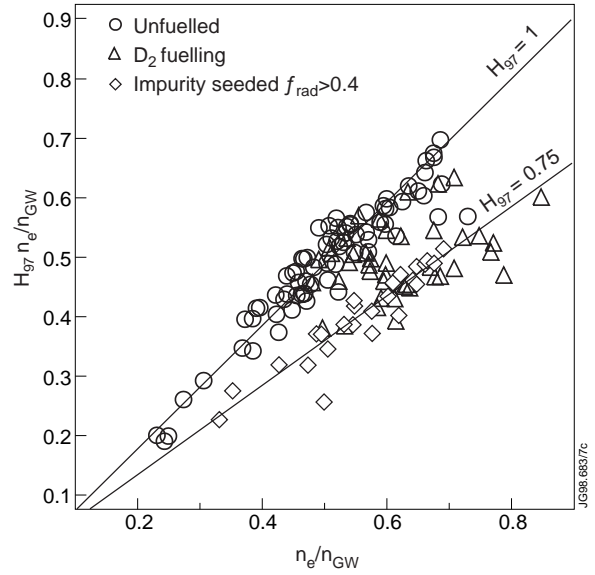


Fig. 7 Normalised  $n_e \tau_E$  versus normalised density for unfueled, impurity seeded and  $D_2$  fuelled H-modes in the JET Mark I and Mark IIA divertors for  $I_p=1.9-2.9$  MA and triangularity  $\delta < 0.24$ .

## 2.5. Confinement at high density and high radiated power

For a given input power, it is observed in JET [9] and other tokamaks that gas fuelling of ELMy H-mode discharges to high density leads to degradation in the global particle confinement time and an effective density limit (the Greenwald density [24]). However, before this limit is reached, the energy confinement time also falls below the level which might be expected from the ITERH-97Py scaling. Figure 6 shows data from both deuterium and tritium gas puffed discharges at 2.6 T/2.6 MA heated with 11-12 MW of NB heating power. The energy confinement time is seen to fall significantly below the ITERH-97Py value when the plasma density exceeds 0.75 of the Greenwald limit; the maximum density achieved is 0.85 of the Greenwald limit. While there is no theoretical basis for the Greenwald density scaling, it is expedient to identify ITER operating conditions with a density consistent with this limit. In fact, it has been possible to extrapolate the ITER demonstration pulses obtained on JET to ITER operation at the higher plasma current of 24 MA (and correspondingly lower  $q_{95}=2.76$ ). In this case, ignition is predicted at the 1.05 GW level for a gyroBohm extrapolation (or  $Q=7.3$  for a Bohm extrapolation), and the required density is close to the Greenwald limit for these conditions.

JET discharges with neon or nitrogen seeded impurities which result in a total radiated power  $>40\%$  of the input power are characterised by Type III ELMs and show energy confinement times which scale as ITERH-97Py, but are lower in magnitude by 25% (Fig. 7) [9].

## 2.6. Confinement degradation due to neoclassical tearing modes

The long pulse ELMy H-mode ITER demonstration pulses obtained during DTE1 at medium to high  $\beta_N$  (between 2 and 3) exhibit modes with a toroidal mode number which is predominantly  $n=2$  and with both  $m=2$  and  $m=3$  components [10]. The modes are mostly triggered by a large sawtooth crash and persist until the NB heating power is switched off. Soft X-ray camera and fast ECE electron temperature measurements show the signature of an island at a major radius  $R=3.5$  m (close to the  $q=1.5$  surface) where the electron temperature profile is flattened locally (Fig. 8). The mode is largest inside the  $q=1.5$  surface, extends up to the magnetic axis, and is relatively small outside the  $q=1.5$  surface. There is good agreement between the measured evolution of the magnetic perturbation associated with the island and the predictions of neoclassical theory. These modes have been identified as neoclassical tearing modes. They result in a reduction in the global energy confinement by 10-20%. It should be noted that although these modes can appear above a normalised plasma pressure of about  $\beta_N=2$ , long pulse ELMy H-mode discharges without continuous  $n=2$  activity also exist up to  $\beta_N \approx 2.6$ . In fact, discharges with  $\beta_N \approx 4$  have

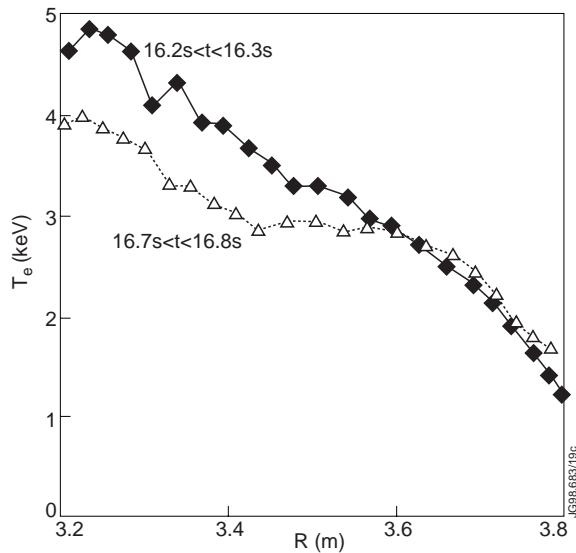


Fig. 8 Flattening of the electron temperature profile near the  $q=1.5$  surface after a sawtooth.

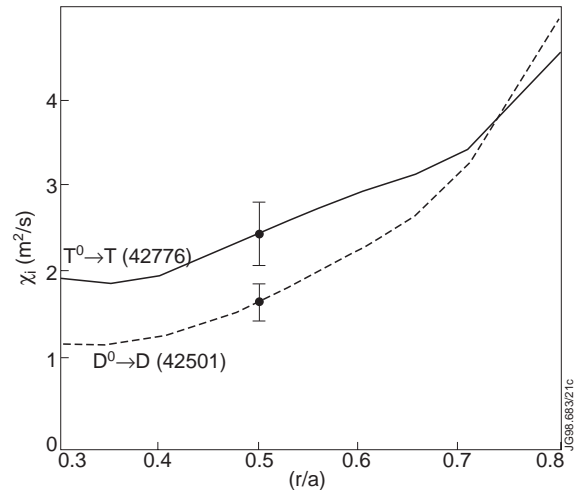


Fig. 9 Ion thermal diffusivities versus normalised plasma radius for ELMy H-mode discharges in deuterium and tritium.

been sustained on JET for up to 5 s. Under these conditions, the modes observed are  $m/n=1/1, 2/2, 3$  neoclassical modes and ELMs.

The data from  $\approx 40$  discharges with  $n=2$  modes show a strong dependence of the critical  $\beta_N$  for the onset of the mode with  $\rho^*$  and a weaker dependence on  $\nu^*$  which is of opposite sign to that of the DIII-D scaling [29], probably reflecting the lower values of  $\nu_i/(\epsilon\omega^*) < 0.1$  in the JET data.

## 2.7. Local transport analysis

The different scalings for the pedestal and core energies (Section 2.4, [8]) are confirmed by trace tritium experiments [30] and by local transport analysis using the TRANSP code. Figure 9 shows the ion thermal diffusivities as a function of normalised plasma radius for similar ELMy H-mode discharges in pure deuterium and pure tritium. It is clear that the mass dependence is different in the plasma core and edge, with the core data being consistent with the gyroBohm scaling ( $A^{0.5}T^{3/2}B^{-2}$ ). Furthermore, a local transport analysis of dimensionless scaling experiments in the radiative regime [9] has confirmed that, provided the effect of variations in collisionality can be ignored, the scaling of the effective thermal

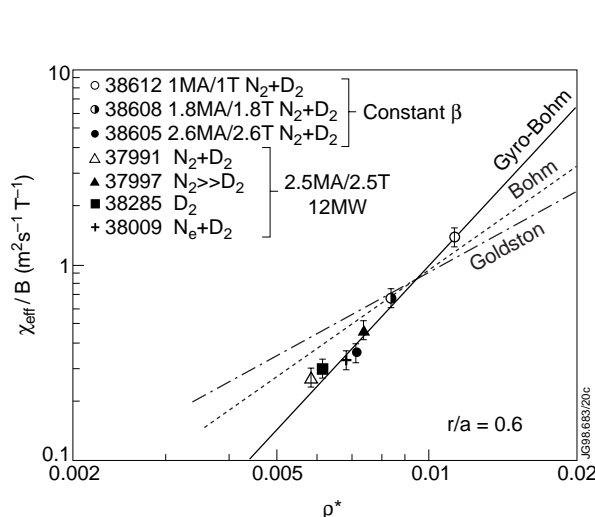


Fig. 10 Logarithmic plot of  $\chi_{eff}/B$  (TRANSP) versus  $\rho^*$  at  $r/a=0.6$  for a variety of impurity seeded and deuterium fuelled discharges. Pulses Nos. 38612, 38608 and 38605 form a  $\rho^*$  scan at constant  $\beta$  ( $\nu^*$  varies).

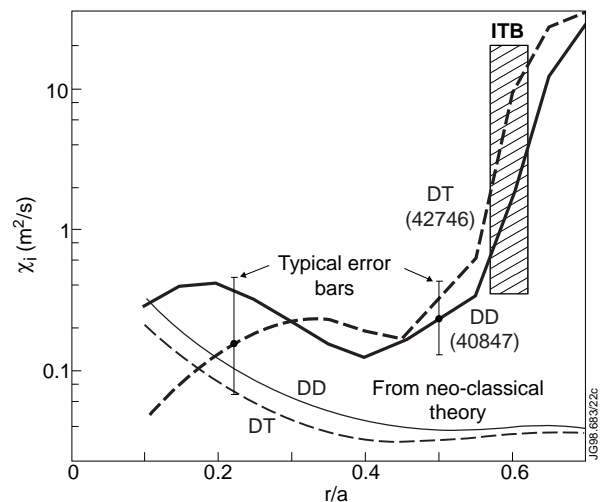


Fig. 11 Ion thermal diffusivities versus normalised plasma radius for optimised shear discharges in D-D and D-T and comparison with neoclassical values.

diffusivity in the core is also consistent with gyroBohm scaling (Fig. 10). Similar conclusions can be drawn from TRANSP analyses of hot ion ELM-free H-modes, while optimised shear discharges [31] show that the ion thermal diffusivity is reduced within the ITB, and can even approach neoclassical [32] levels (Fig. 11).

### 3. D-T PERFORMANCE AND RELATED PHYSICS

The most important results of DTE1 relate to fusion performance in ELMy and ELM-free H-modes [12], to the physics issues of ICRF heating in D-T [16], alpha particle heating and Alfvénic instabilities [17] and the first demonstration of the optimised shear mode in D-T [18, 19].

#### 3.1. Fusion energy, power and gain

##### 3.1.1. ELMy H-mode

During DTE1 the best ever fusion performance in an ELMy H-mode was produced at 3.8 MA/3.8 T. Steady-state conditions were maintained by regular Type I ELMs, resulting in the production of a fusion energy of 21.7 MJ and a ratio of the fusion energy to the input energy of 0.18 over 3.5 s ( $\approx 8$  energy confinement times). A fusion power of 4 MW was maintained for  $\approx 4$  s.  $\beta_N$  was limited to 1.3 by the available additional heating power (23 MW of combined NB (90%) and ICRF (10%) heating); fusion performance was limited by the density being too high and the temperature too low.

##### 3.1.2. Hot ion ELM-free H-mode

The hot ion ELM-free H-mode is the traditional mode for high performance in JET plasmas [33] and prior to DTE1 reproducible discharges were obtained reliably in D-D. With good mixture control, this performance during DTE1 led to records of fusion power and fusion gain. Five high power ELM-free H-mode discharges produced more than 12 MW of fusion power. Figure 12 shows the pulse with the highest fusion power of 16.1 MW. This was obtained with 25.7 MW of input power, comprising 22.3 MW of NB heating combined with 3.1 MW of hydrogen minority ICRF heating. As with hot ion ELM-free discharges in deuterium, the D-T discharges were transient, with the stored energy, fusion power and electron density rising monotonically with time until limited by MHD activity (see structure in Balmer alpha signal): first an external kink mode and then a giant ELM [34]. Following detection of the giant ELM, the heating power is switched off to save neutrons. The ion temperature peaks at  $\approx 28$  keV, significantly higher than the electron temperature which is  $\approx 14$  keV. As shown in Fig. 12, this pulse reaches a record fusion gain  $Q_{in}=P_{fus}/P_{in}=0.62$  and  $Q_{tot}=P_{fus}/(P_{loss}-P_{\alpha})=0.95\pm 0.17$  [5], the value which  $Q_{in}$  would reach if the same plasma conditions could be obtained in steady-state.

These experiments show no deleterious isotopic effect from the use of tritium, or alpha particle effects on stability or confinement. They confirm that, provided the D-T mix can be optimised (as in this case), D-T performance can be predicted on the basis of D-D experience, even in the presence of alpha particle heating powers greater than 10% of the input power, confirming both the quality of the JET kinetic data and the physics contained within the JET analysis codes. Indeed, the D-D to D-T fusion power multiplier (210) is close to that expected from the respective rate coefficients [5].

#### 3.2. Ion cyclotron resonance frequency heating of D-T plasmas

Ion Cyclotron Resonance Frequency (ICRF) heating is one of the main heating methods foreseen for a tokamak fusion reactor and, during DTE1, the physics and performance of four ICRF heating schemes for D-T operation were tested successfully [35]. Furthermore, most of the results obtained in these ICRF heating experiments are in excellent agreement with PION code predictions [16].

##### 3.2.1. Ion heating with deuterium and helium minority concentrations

Deuterium minority heating at the fundamental resonance of deuterium ( $\omega_{cD}$ ) in tritium plasmas was demonstrated for the first time on JET [35]. The plasma density and the deuterium minority concentration (up to 20%) were optimised for maximum fusion power from reactions between suprathreshold deuterons and thermal tritons. For a pulse with 9% deuterium and 91% tritium, an ICRF heating power of 6 MW produced a peak fusion power of 1.66 MW. This steady-state discharge had a fusion gain of over

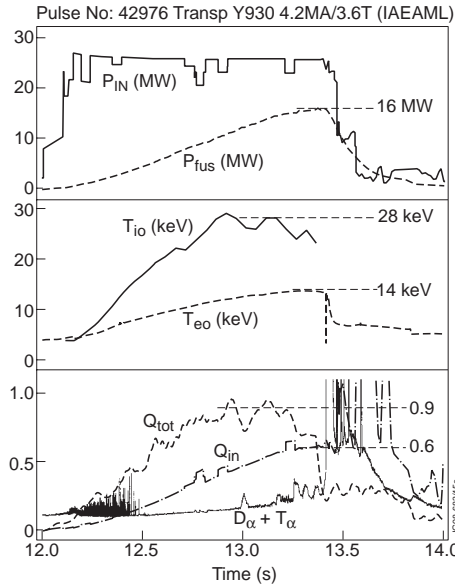


Fig. 12 Various time traces for the highest fusion yield hot ion H-mode discharge. From top to bottom: input and fusion power; central ion and electron temperatures; ratios of fusion to loss power minus alpha particle heating power,  $Q_{tot}$ , and of fusion to input power  $Q_{in}$  and  $D_{\alpha} + T_{\alpha}$  intensity.

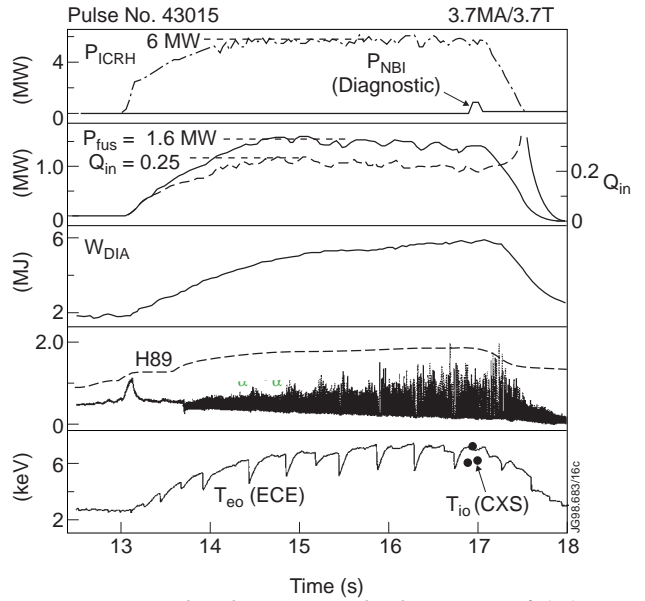


Fig. 13 H-mode plasma in which 6 MW of (D)T ICRF heating power gave 1.66 MW of fusion power and  $Q_{in}=0.22$  was obtained in quasi steady-state.

0.22 for three plasma energy confinement times (2.7s) (Fig. 13). A deuteron energy of 125 keV was determined from the Doppler broadening of the neutron spectrum. This is both optimum for fusion reactions and close to the critical energy of thermalising fast ions, resulting in high fusion efficiency and strong bulk ion heating.

Strong bulk ion heating was also observed with  $^3\text{He}$  minority heating at the fundamental resonance of  $^3\text{He}$  ( $\omega_{C3\text{He}}$ ) in approximately 50:50 D:T plasmas with 5-10%  $^3\text{He}$ . The neutron spectrum shows that the fusion reactions were thermal with central ion and electron temperatures of 13 keV and 12 keV, respectively. This scheme seems to be the most promising ICRF heating scheme for achieving ignition in ITER [36]. As heating progresses, the  $^3\text{He}$  concentration could then be reduced as second harmonic tritium ion heating begins to dominate (Section 3.2.2.).

### 3.2.2. Electron heating using the second harmonic of tritium

Second harmonic tritium and fundamental  $^3\text{He}$  minority ICRF heating are competing absorption mechanisms, since both resonances occur at the same position in the plasma. Heating at the second harmonic of tritium ( $2\omega_{cT}$ ) in a 50:50 D:T plasma produces energetic tritons well above the critical energy, resulting in  $\approx 90\%$  of the input power being coupled to the electrons. The fusion power was typically a factor of four lower than with  $^3\text{He}$  minority heating under similar conditions, but was predominantly from thermal reactions. In ITER, predictions indicate that mainly ion heating will occur since the power density per particle will be considerably lower, resulting in triton tail ions with lower energies. In addition, all fast ions will be confined in ITER, making it an efficient bulk ion heating scheme.

### 3.3. Alpha particle heating

To separate the alpha particle heating from possible isotope effects on energy confinement, a series of specially designed discharges was carried out in which the D-T mixture was varied from pure deuterium to almost pure tritium while all other parameters including the external heating power ( $\approx 10.4$  MW NB heating) were kept as constant as possible [17, 37]. Comparing the pure deuterium and almost pure tritium data demonstrated (Fig. 14) that the global energy confinement time in ELM-free H-modes has no or little dependence on isotope. The slight increase in confinement near 50:50 D:T

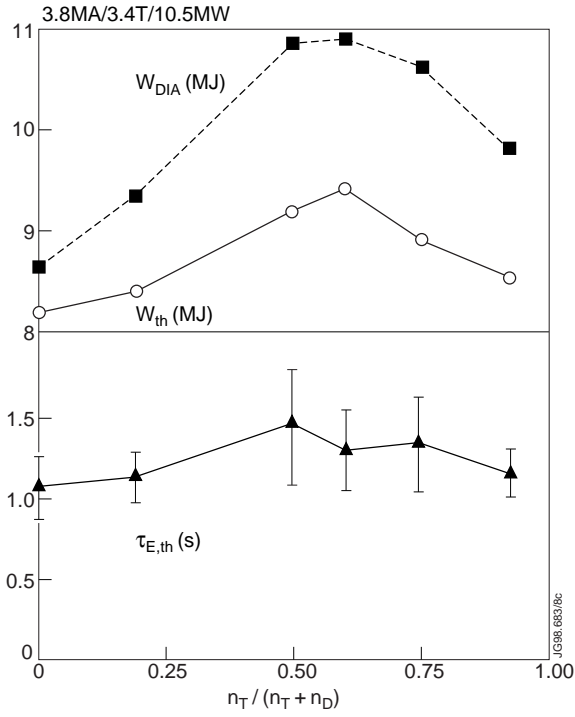


Fig. 14 Diamagnetic and thermal plasma energy (top) and thermal energy confinement time (bottom) versus tritium concentration.

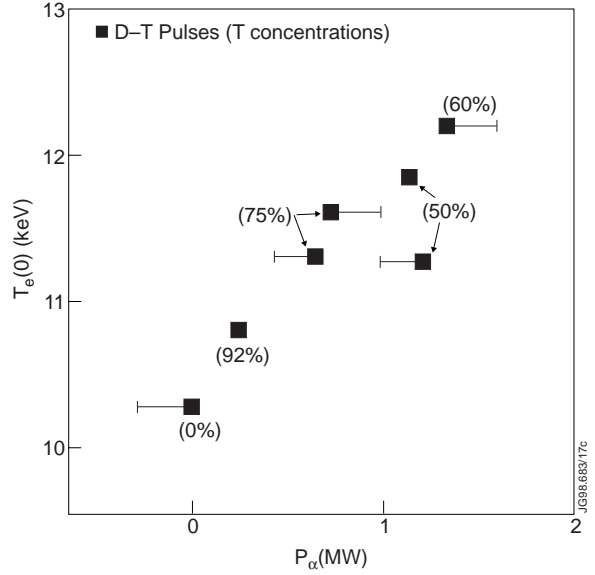


Fig. 15 Central electron temperature versus alpha particle heating power. The bars indicate the variation in NB power compared to the 92% tritium reference pulse. The figures in brackets are the tritium concentrations.

mixtures is, at least in part, the result of the peaked alpha particle heating which increased the power transferred to the electrons in the centre by  $\approx 60\%$ . The strong correlation between the maximum diamagnetic and thermal plasma energies and the optimum D-T mixture (Fig. 14) is a clear demonstration of alpha particle heating. This is seen even more clearly in Fig. 15 where the central electron temperature is plotted against the calculated alpha particle heating power for a selection of the pulses in the D-T mixture scan. The highest electron temperature shows a clear correlation with the maximum alpha particle heating power and with the optimum D:T plasma mixture (40:60). A regression fit to the data gives a change in central electron temperature of  $1.3 \pm 0.23$  keV with 1.3 MW of alpha particle heating. Furthermore, the alpha particle heating was as effective as hydrogen minority ICRF heating in deuterium plasmas under similar conditions which, like alpha particle heating, couples predominantly to electrons. This is a strong indication that the confinement and slowing down of the alpha particles and their associated heating are classical and, that in the absence of alpha particle driven TAE instabilities (Section 3.4), there are no unexpected effects which might prevent ignition in ITER or a reactor.

### 3.4. Alpha particle driven Alfvénic instabilities

Toroidal Alfvén Eigenmodes (TAEs) have been observed in JET when fast particles involved in plasma heating (eg. fast ions from ICRF or NB heating) slowing down from their birth energy resonate with Alfvén waves. There is the potential for particle and energy losses which could damage vessel components. During DTE1, TAEs have been identified in the magnetic fluctuation spectra with, for example,  $2\omega_{CT}$  ICRF heating above an RF power of 5 MW [38]. Experiments performed with tritium NB injection into tritium plasmas, deuterium into deuterium, and hydrogen into hydrogen provide an important confirmation of the models for TAE growth rate [17]. On the other hand, no alpha particle driven TAEs were excited in the record fusion power D-T discharges, in agreement with calculations which show that the normalised alpha particle pressure in these discharges is a factor of two below the threshold for alpha particle driven instabilities [39].

### 3.5. First demonstration of optimised shear mode in D-T

#### 3.5.1. Formation of internal transport barriers

The principal feature of the optimised shear scenario [13, 14, 40-42] is the formation of an Internal Transport Barrier (ITB). These have now been established for the first time in D-T [31], and for a range of magnetic fields and divertor geometries. Power and current profile control are used to establish an ITB, to delay the transition to an H-mode phase, and to avoid a  $\beta$  limit disruption. The formation of an ITB is very sensitive to the  $q$  profile. The scenario comprises the formation of a target plasma by pre-heating during a fast current ramp, using lower hybrid waves to assist breakdown and to provide some current drive, followed by ICRF pre-heating to slow current penetration. When the current profile is such that the volume within the  $q=2$  surface is reasonably large ( $r/a \approx 0.3-0.4$ ), high power, typically 16-18 MW of NB heating together with 6 MW of ICRF heating, is applied.

After some scenario development, largely because of the lower H-mode threshold power (the early appearance of ELMs prevented the formation of an ITB) and because the  $q$  profile was different in D-T, strong ITBs were established in D-T and with a threshold power and current profile not markedly different from that in D-D [31].

When an ITB forms, substantial increases in plasma density and temperature occur during the first second of high power heating. As shown in Fig. 16, the temperature gradient can reach 150 keV/m and the pressure gradient 1 MPa/m. The input power is controlled by feedback on the neutron rate in order to avoid excessive pressure gradients which provoke MHD instabilities. As a result, the plasma can be maintained close to the ideal MHD stability limits for most of the heating pulse, as shown in Fig. 17 for optimised shear discharges in D-D and in D-T [43]. In both cases,  $\beta_N$  increases as the ITB moves outwards with time to  $\approx 2/3$  of the plasma radius and the pressure profile becomes less peaked. Towards the end of the discharge, an H-mode forms, reducing further the peaking factor, moving the discharge away from the instability boundary but also leading to the subsequent termination of the discharge by disruption. The highest performance has been achieved with small or slightly reversed central shear and  $q(0)$  in the range 1.5-2. In D-T, as in D-D, the foot of the steep gradient region was located just inside the  $q=2$  surface and both moved outwards with time. This is confirmed by TRANSP simulations, which also show that more than half of the full plasma current at peak performance was driven non-inductively, with the bootstrap and NB driven currents being about equal and localised close to the centre.

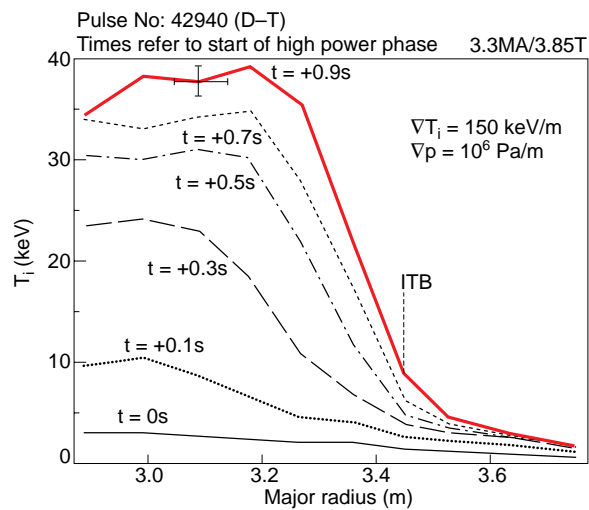


Fig. 16 Ion temperature profiles at various times after the start of high power heating in an optimised shear discharge showing the formation of an Internal Transport Barrier (ITB).

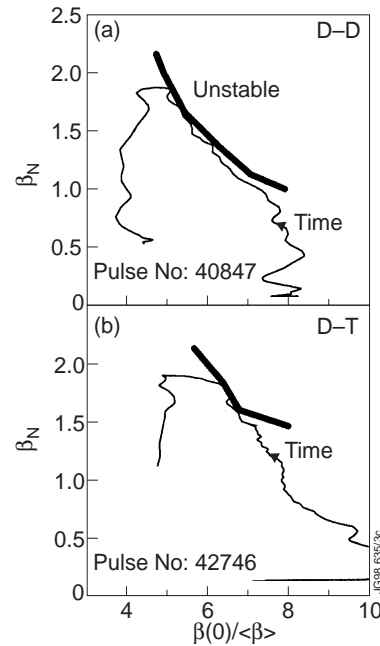


Fig. 17 Stability diagrams for optimised shear discharge, (a) in D-D and (b) in D-T.

The neutron and time constraints on DTE1 did not allow these discharges to be fully optimised. Nevertheless, 8.2 MW of fusion power was produced (Fig. 18), even though the central tritium concentration ( $\approx 34\%$ ) and central density ( $3.9 \times 10^{19} \text{ m}^{-3}$ ) were relatively low, the ion temperature ( $\approx 33 \text{ keV}$ ) was too high for maximum fusion reactions, and the power control was inadequate to prevent a terminal disruption.

### 3.5.2. Modelling of optimised shear discharges

The basic transport model used at JET for a number of years comprises a combination of Bohm and gyroBohm anomalous transport combined with neoclassical ion transport. The Bohm transport is assumed to result from toroidal coupling of long wavelength turbulence (non-local) and the gyroBohm transport to be produced by short wavelength turbulence which is only weakly affected by toroidicity (local). This model has been applied successfully to a range of L-mode, ELMy H-mode and ELM-free H-mode discharges in the JET and ITER data bases, but it requires modification in order to simulate the formation of an ITB as observed in the optimised magnetic shear discharges. With the assumption that the suppression of the long wavelength turbulence is sufficient to allow the formation of an ITB, the Bohm coefficient is multiplied by a step function which depends on control parameters related to turbulence stabilisation by shear in the plasma rotation and to turbulence decorrelation due to toroidicity in a region with small magnetic shear [27].

Figure 19 shows the result of applying this model to Pulse No. 40847. Good agreement is obtained for the time evolution of the temperature profile when it is assumed that the Bohm transport is suppressed everywhere inside the region where the switch-off condition is satisfied. On the other hand, a model which does not include shear in the plasma rotation fails to produce a transport barrier, while the gradual radial expansion of the transport barrier cannot be reproduced without the stabilising term due to

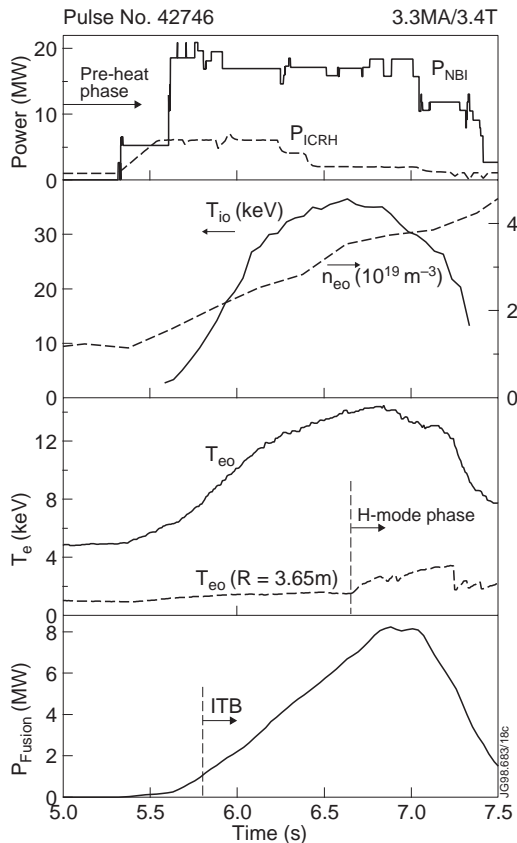


Fig. 18 Various time traces for the optimised shear discharge with the highest fusion yield. From top to bottom: NB and ICRF heating power; central ion temperature and electron density; central and edge electron temperature; and fusion power.

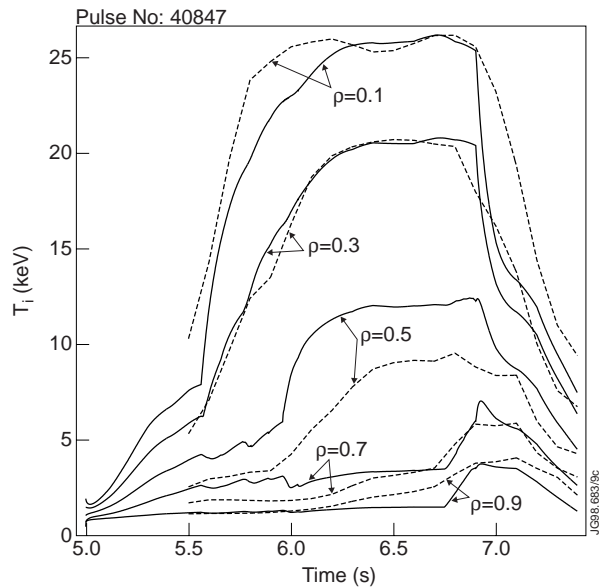


Fig. 19 Time evolution of measured (solid lines) and simulated (dashed lines) ion temperatures at different radii for optimised shear Pulse No. 40847, showing the development and erosion of an ITB.

magnetic shear. Furthermore, this model which reproduces the formation of the ITB and the transition to improved core confinement, also describes the erosion and disappearance of the ITB soon after the L-H transition since the rapid rise in edge pressure reduces the shear in the core plasma rotation.

### 3.5.3. Development towards steady-state with double transport barriers

The highest fusion performance in optimised shear discharges was normally obtained by prolonging the phase during which the plasma edge was in L-mode [13-14]. A significant number of discharges, however, developed both an ITB and an ELMy H-mode edge as illustrated in Fig. 20, and still produced a substantial fusion yield. In the discharge shown in Fig. 20, an ITB is formed and the central ion temperature reaches 24 keV, while the edge ion temperature is about 3 keV, typical of an ELMy H-mode. In fact, the ELMy H-mode edge prevents excessive pressure peaking and improves MHD stability.

In this pulse the fusion power increases from the start of the main heating phase until it reaches 6.8 MW, at which time the input power was reduced to economise on D-T neutrons. This increase in fusion yield is due to a continuous build-up of central density together with an increase of the tritium concentration. The stored plasma energy reaches 8.8 MJ for a total input power of 18.4 MW and a corresponding confinement enhancement factor  $H_{89} \approx 2.3$  relative to the ITER89-P scaling [44]. In this pulse, as in similar D-T and D-D pulses, the positions of the  $q=2$  magnetic surface and the ITB change only slowly with time. This can be interpreted as a consequence of the generation of an edge bootstrap current. At 6.3 s, the power was stepped down and it is interesting to note that the subsequent collapse of the ITB triggers an ELM-free H-mode.

A comparison of such a double barrier (ITB plus ELMy H-mode) discharge with a conventional ELMy H-mode discharge without an ITB in the same plasma configuration and with similar input power (22.5 MW) shows the advantage of the double barrier plasma: the fusion triple product  $n_i(o)T_i(o)\tau_E$  reaches  $4.4 \times 10^{20} \text{ m}^{-3}\text{keVs}$  compared to  $1.9 \times 10^{20} \text{ m}^{-3}\text{keVs}$ , and the fusion gain is 0.4 compared to 0.2 [19]. In addition, the ELMs are much smaller in amplitude in double barrier discharges (the energy loss in a single ELM is typically a factor of ten smaller) which is of great significance because of the critically high peak power loads on the divertor target plates in a standard ELMy H-mode ignited ITER scenario.

Although this route could not be explored further during DTE1 because of the imposed neutron constraint, such discharges show significant promise for steady-state high fusion yield; better control of the plasma edge and/or the current profile will however, be required.

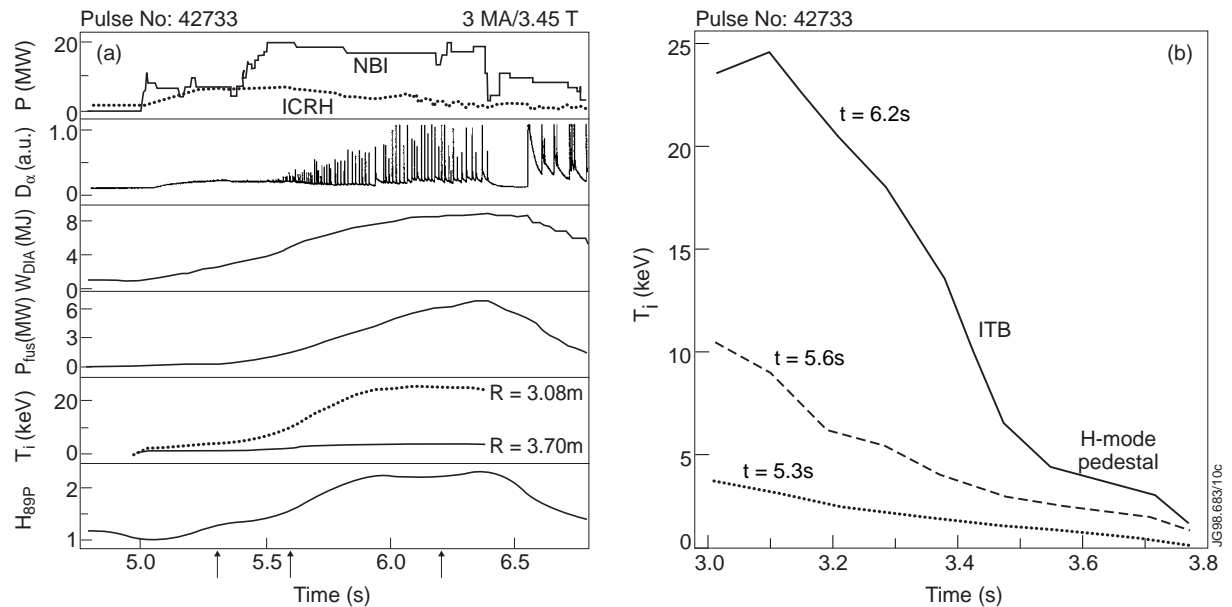


Fig. 20 (a) Various time traces and (b) ion temperature profiles for a pulse which develops an internal transport barrier simultaneously with an ELMy H-mode barrier. The power was stepped down at 6.4s to limit the number of D-T neutrons produced.

### 3.5.4. Projections to future JET operations

The potential of optimised shear discharges for future D-T operation on JET has been explored with JETTO transport code calculations combined with MHD stability analyses [19]. LHCD is essential to establish and maintain a wide core region of slightly negative shear, and with  $\approx 3.5$  MW of LHCD, ballooning modes are suppressed and  $\beta_N$  can be raised from 2.4 to 3.0. Fusion power in the range 20-30 MW and  $Q_{in}$  in excess of unity are predicted at 3.9 MA/ 3.4 T with the existing heating and current drive systems, and even higher performance with modest upgrades. However, there are significant uncertainties in the particle transport, and these leave a wide margin in the predictions.

## 4. TRITIUM SUPPLY, CONCENTRATIONS AND IN-VESSEL INVENTORY

During DTE1, tritium was supplied, collected from the exhaust gases and processed by an industrial scale tritium processing plant which worked in a closed-cycle with the tokamak, pumping the torus in continuous operation. This allowed the site inventory of 20 g of tritium to be processed repeatedly; 99.3 g of tritium was supplied to the JET machine, requiring eight processing cycles in which the tritium was routinely separated to better than 99.4% purity. The tritium gas was either injected directly into the torus via a gas valve (a total of 35 g) or by NB injection. In the latter case only a small fraction of the tritium gas supplied to the NB box was injected into the torus via the high energy tritium neutral beams. The remaining tritium gas was trapped by the NB cryopumps and was recovered to better than 98% accountability in nightly regenerations.

Tritium concentrations in the plasma could be relatively easily controlled by loading the walls to an appropriate level of tritium using ohmic or low power ICRF heated discharges. Tritium concentrations greater than 90% were readily obtained. Furthermore during DTE1 and the ensuing clean-up phase, tritium concentrations in the plasma and exhaust gases were reduced at a rate similar to the experience from the PTE [45].

On the other hand, the in-vessel tritium inventory developed quite differently from that in the PTE. During the DTE1 campaign about 30% of the cumulative tritium input remained in the torus and this was reduced to about 17% ( $\approx 6$  g) following extensive operation in hydrogen and deuterium; this was more than three times larger than had been expected from the tritium retention results of the PTE. This high level of tritium retention during and after DTE1 is thought to be related to carbon films, saturated with deuterium and tritium and found in cold regions of the divertor [45]. While most of the JET vessel was heated to 320°C, these cold regions, shadowed from direct contact with the plasma, were cooled to  $\approx 50^\circ\text{C}$ , allowing stable films to form with more than 40% hydrogen concentrations in carbon. In contrast, at the time of the PTE, i.e. before the installation of a divertor, the whole vessel was maintained at 300°C. Extrapolation of these tritium retention results to ITER would result in unacceptably high tritium inventories; the ITER divertor needs to be re-designed to take this fully into account.

## 5. FIRST RESULTS WITH THE MARK IIGB DIVERTOR

### 5.1. Divertor studies

First results with the recently installed Mark IIGB divertor [20] indicate that the particle exhaust and neutral compression continue to rise as the divertor becomes increasingly more closed. Furthermore, it has been possible, for the first time, to use differential deuterium fuelling to modify the in-out symmetry of the divertor plasma. Figure 21 shows that inner divertor fuelling causes an early onset of detachment and the density limit, while outer divertor fuelling produces more equal ion fluxes to each divertor, delays the onset of detachment and leads to a higher density limit. This behaviour may be due to the presence of the septum.

### 5.2. Optimised shear studies

Optimised shear discharges with ITBs have also been produced with the newly installed Mark IIGB divertor. The minimum power (combined NB and ICRF heating) required to trigger an ITB shows an almost linear dependence on magnetic field (Fig. 22) for similar conditions of target density,  $q$  profile (target  $q(0)$  being close to 2) and small ELMs at the edge. There is a greater tendency towards the

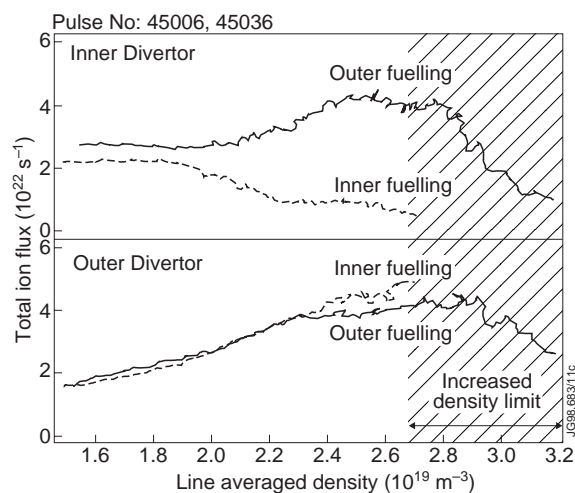


Fig.21 Differential gas fuelling modifies the symmetry of the divertor plasma parameters, leading to a higher density limit.

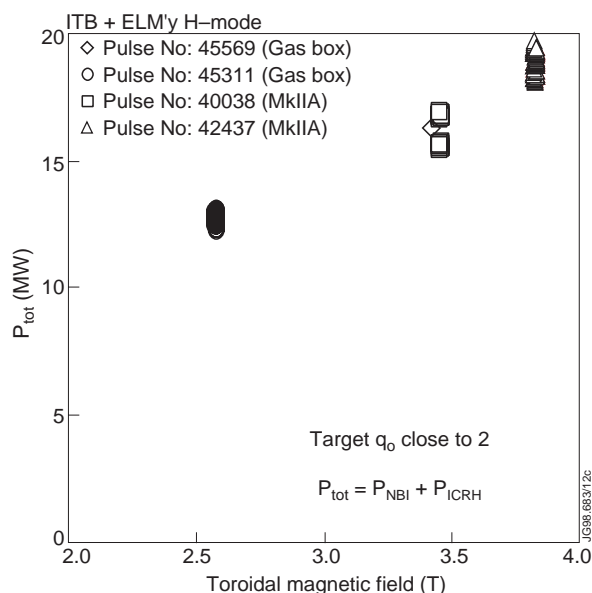


Fig. 22 Minimum total heating power (NBI+ICRH) required to trigger an ITB versus magnetic field. Pulses indicated are representative of pulses where an ITB is produced at low power.

formation of double barrier plasmas with grassy ELMs [19]. Tight control of the  $q$  profile is required during the whole of the double barrier phase so as to avoid degradation related to the location of rational  $q$  surfaces. With off-axis LHCD, the evolution of the  $q$  profile during the high performance phase can be slowed down, limiting the contraction of the region of low magnetic shear after the current ramp-up phase. Experiments which use a puff of krypton gas to radiate the power crossing the separatrix are shown in Fig. 23. With a total input power of up to 22 MW, grassy ELMs are seen which disappear and an ITB forms when the radiated power reaches 8-10 MW. Later in the discharge the ELMs reappear, and the input power (which has been stepped down) is insufficient to maintain the ITB.

## 6. SUMMARY AND CONCLUSIONS

JET experiments since the 1996 IAEA Conference in Montreal reached a zenith with D-T operation in 1997 and continued with an ITER physics campaign, the installation of the Mark IIGB “Gas Box” divertor using full remote handling techniques, and the start of operation with this more closed divertor. These experiments have produced a wealth of unique and pertinent physics results, pointing the way towards an improved theoretical understanding and allowing more accurate predictions for ITER.

The standard ITER operating mode (steady-state ELMy H-mode) has been well characterised empirically and dimensionless scaling “Wind Tunnel” experiments can be extrapolated to ignition with ITER parameters. The scaling is close to gyroBohm, but does not have the correct mass dependence. The separation of the thermal energy of the plasma into core and pedestal contributions, confirmed by local transport analysis, could explain this discrepancy and bring a theoretical understanding of energy confinement within reach. The gyroBohm nature of the core transport observed in each mode of high confinement has allowed high fusion performance plasmas to be produced and studied during DTE1 and would be beneficial to ITER. The scale length of the edge transport barrier is crucial, also for extrapolating the pedestal energy to ITER.

Figure 24 summarises the development of fusion power over the last six years in JET and TFTR. It encompasses the first ever high fusion power (1.7 MW) pulse with 11% tritium in JET in 1991 [11], the pulse with the highest fusion power (10.7 MW) from the 50:50 D-T experiments on TFTR during the period 1993 to 1997 [3], and finally the record pulses from the JET D-T experiments in 1997 (DTE1) [5]: 16.1 MW in an ELM-free H-mode, 8.2 MW in the optimised shear mode of operation, and 4 MW in a steady-state ELMy H-mode discharge.

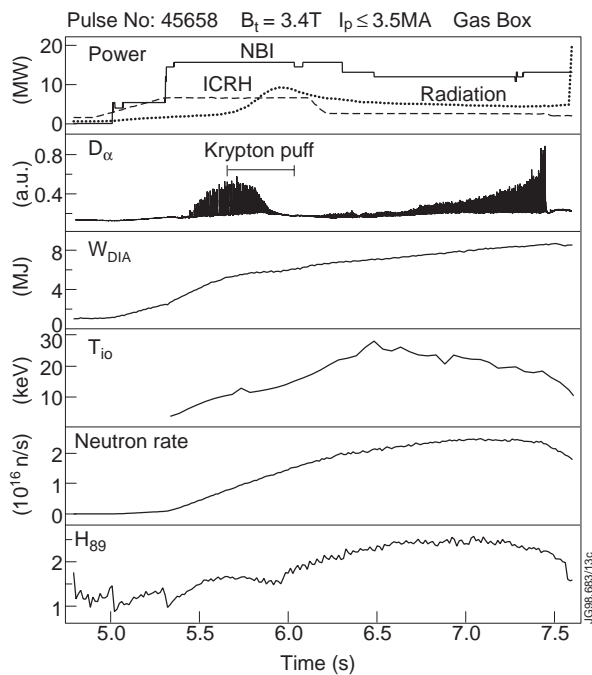


Fig. 23 Time evolution of typical signals for Pulse No. 45658 in D-D at 3.4T. The plasma current reaches 3.5 MA at 7 s. Krypton gas is puffed at 5.8 s for 0.2 s.

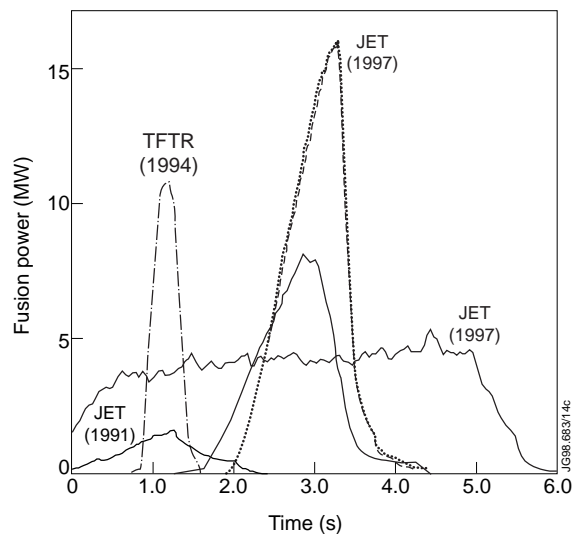


Fig. 24 Fusion power development in JET (1991 and 1997) and TFTR (1993 to 1997).

Radio frequency heating of D-T plasmas is well understood and most effects are well simulated by theory. The results can be extrapolated to effective bulk ion heating on the way to ignition in ITER. Alpha particle heating has been clearly observed and is consistent with classical expectations, thus confirming the process by which ignition would occur in a reactor. Linear stability calculations of TAEs are in good agreement with experimental results, but the saturation of these modes and their effect on transport has yet to be observed.

The advanced operating mode (optimised shear) has been obtained in D-T, at different magnetic fields and with different divertors. It takes confinement towards the most favourable theoretical expectations (i.e. ion heat conduction approaching neoclassical levels) and the plasma pressure is limited in accord with theory. A transport model which simulates the formation of the transport barrier and its subsequent erosion following an L-H transition has been proposed. The basis for performance optimisation (high plasma pressure, long pulse) using profile control is thus improved.

The Mark IIGB campaign has started and is already producing significant results. In the area of divertor physics, the in/out symmetry of the divertor plasma has been modified for the first time using differential gas fuelling, leading to higher density limits. The septum has also been used successfully as a pumped limiter, opening up a new line of research for JET. In the area of high performance operation, optimised shear discharges have been re-established, LHCD has been used to modify the current profile in the high performance phase of the discharge and the puffing of krypton gas into optimised shear discharges has been very effective in restoring L-mode edge conditions and helping to establish an ITB.

The new and exciting results already obtained with the Mark IIGB divertor testify that JET, with its unique combination of divertor configuration, heating and profile control systems and tritium capability, should remain, for many more years, the most valuable machine in support of ITER or any other Next Step tokamak.

## ACKNOWLEDGEMENTS

The presenter wishes to thank all his colleagues at JET who have made these significant achievements possible and in particular to remember Drs. B E Keen and D F H Start who died earlier this year and whose contributions to the JET Project were immeasurable.

## REFERENCES

- [1] JET TEAM (presented by J. JACQUINOT), in Fusion Energy 1996 (Proc. 16th Int. Conf. Montreal, Canada, 1996) Vol. 1, IAEA, Vienna (1997) 57.
- [2] AYMAR, R., CHUYANOV, V., HUGUET, M., PARKER, R., SHIMOMURA, Y. and the ITER Joint Central Team and Home Teams, in Fusion Energy 1996 (Proc. 16th Int. Conf. Montreal, Canada, 1996) Vol. 1, IAEA, Vienna (1997) 3.
- [3] McGUIRE, K. M. et al., in Fusion Energy 1996 (Proc. 16th Int. Conf. Montreal, Canada, 1996) Vol. 1, IAEA, Vienna (1997) 19.
- [4] GIBSON, A. and the JET TEAM, Physics of Plasmas **5** (1998) 1839.
- [5] KEILHACKER, M. et al., and the JET TEAM, "High Fusion Performance from Deuterium-Tritium Plasmas in the JET Tokamak", accepted for publication in Nucl. Fusion (1998).
- [6] JACQUINOT, J. et al., and the JET TEAM, "Overview of ITER Physics Deuterium-Tritium Experiments in JET", accepted for publication in Nucl. Fusion (1998).
- [7] ITER Confinement Database and Modelling Working Group (Presented by J.G. CORDEY), Plasma Phys. Control. Fusion **39** (1997) B115.
- [8] JET TEAM (presented by J.G. CORDEY), IAEA-F1-CN-69/EX7/1, this conference.
- [9] JET TEAM (presented by G.F. MATTHEWS), IAEA-F1-CN-69/EX3/5, this conference.
- [10] JET TEAM (presented by G.T.A. HUYSMANS), IAEA-F1-CN-69/EXP3/3, this conference.
- [11] JET TEAM, Nucl. Fusion **32** (1992) 187.
- [12] JET TEAM (presented by F.G. RIMINI), IAEA-F1-CN-69/EXP1/8, this conference.
- [13] JET TEAM (presented by C. GORMEZANO), in Fusion Energy 1996 (Proc. 16th Int. Conf. Montreal, Canada, 1996) Vol. 1, IAEA, Vienna (1997) 487.
- [14] JET TEAM (presented by F. X. SÖLDNER), Plasma Phys. Control. Fusion **39** (1997) B353.
- [15] JET TEAM (presented by M.A. PICK), IAEA-F1-CN-69/FT2/2, this conference.
- [16] JET TEAM (presented by D.F.H. START), IAEA-F1-CN-69/CD1/2, this conference.
- [17] JET TEAM (presented by P.R. THOMAS), IAEA-F1-CN-69/EX1/1, this conference.
- [18] JET TEAM (presented by C. GORMEZANO), IAEA-F1-CN-69/EXP1/5, this conference.
- [19] JET TEAM (presented by F.X. SÖLDNER), IAEA-F1-CN-69/EXP1/6R, this conference.
- [20] JET TEAM (presented by R.D. MONK), IAEA-F1-CN-69/EX6/4, this conference.
- [21] ASDEX TEAM, Nucl. Fusion **29** (1989) 1959.
- [22] JFT2-M GROUP, Proc. 3rd H-mode Workshop **1** (1991) 141.
- [23] JET TEAM (presented by J.P. CHRISTIANSEN), IAEA-F1-CN-69/EXP2/02, this conference.
- [24] GREENWALD, M. et al., Nucl. Fusion **28** (1988) 2199.
- [25] JET TEAM (presented by M. KEILHACKER), Plasma Phys. Control. Fusion **39** (1997) B1.
- [26] TAKIZUKA, T., Plasma Phys. Control. Fusion (Proc. 6th H-mode Workshop, Gut Ising, 1997), to appear.
- [27] JET TEAM (presented by V.V. PARAIL), IAEA-F1-CN-69/EX6/1, this conference.
- [28] SAIBENE, G. et al., in preparation for submission to Nucl. Fusion (1998).
- [29] JET TEAM (presented by K.-D. ZASTROW), IAEA-F1-CN-69/EXP1/07, this conference.
- [30] LA HAYE, R. et al., in Fusion Energy 1996 (Proc. 16th Int. Conf. Montreal, Canada, 1996) Vol. 1, IAEA, Vienna (1997) 747.
- [31] GORMEZANO, C. et al., Phys. Rev. Lett. **80** (1998) 5544.
- [32] HINTON, F.L. and HAZELTINE, R.D., Reviews of Modern Physics **48** (1976) 239.
- [33] JET TEAM (presented by P. J. LOMAS), in Fusion Energy 1996 (Proc. 16th Int. Conf. Montreal, Canada, 1996) Vol. 1, IAEA, Vienna (1997) 239.
- [34] HUYSMANS, G. T. A. et al., Nucl. Fusion **38** (1998) 179.
- [35] START, D. F. H. et al., Phys. Rev. Lett. **80** (1998) 4681.
- [36] START, D. F. H. et al., in Europhysics Conference Abstracts (Proc. 24th EPS Conf. on Controlled Fusion and Plasma Physics, Berchtesgaden, Germany, 1997), Vol 21A, Part 1 (1997) 141.
- [37] THOMAS, P. R. et al., Phys. Rev. Lett. **80** (1998) 5548.
- [38] FASOLI, A. et al., Plasma Phys. Control. Fusion **39** (1997) B287.
- [39] SHARAPOV, S. E. et al., "Stability of Alpha Particle Driven Alfvén Eigenmodes in High Performance JET D-T Plasmas" submitted for publication in Nucl. Fusion (1998).
- [40] KESSEL, C. et al., Phys. Rev. Lett. **72** (1994) 1212.

- [39] STRAIT, E. J. et al., Phys. Rev. Lett. **75** (1995) 4421.
- [40] USHIGUSA, K. and the JT-60 Team, in Fusion Energy 1996 (Proc. 16th Int. Conf. Montreal, Canada, 1996) Vol. 1, IAEA, Vienna (1997) 37.
- [41] HUYSMANS, G. T. A. et al., in Europhysics Conference Abstracts (Proc. 24th EPS Conf. on Controlled Fusion and Plasma Physics, Berchtesgaden, Germany, 1997), Vol. 21A, Part 1 (1997) 21.
- [42] SCHISSEL, D.P. et al., Nucl. Fusion **31** (1991) 73.
- [43] ANDREW, P.L. et al., submitted for publication in J. Nuclear Mater. (Proc. 13<sup>th</sup> Conf. On Plasma Surface Interactions in Controlled Fusion Devices, San Diego, USA, 1998).

## Appendix

### THE JET TEAM

JET Joint Undertaking, Abingdon, Oxon, OX14 3EA, U.K.

J.M. Adams<sup>1</sup>, P. Ageladarakis, B. Alper, H. Altmann, S. Arshad, P. Andrew, Y. Andrew<sup>12</sup>, N. Bainbridge, B. Balet, Y. Baranov<sup>8</sup>, P. Barker, R. Barnsley<sup>2</sup>, M. Baronian, D.V. Bartlett, A.C. Bell, E. Bertolini, C. Bevil, V. Bhatnagar, A.J. Bickley, H. Bindslev, K. Blackler, D. Bond, T. Bonicelli, D. Borba<sup>18</sup>, M. Brandon, H. Brelen, P. Brennan, W.J. Brewerton, M. Brix<sup>4</sup>, M.L. Browne, T. Budd, R. Budny<sup>13</sup>, T. Businaro, C. Caldwell-Nichols, D. Campling, P. Card, C.D. Challis, A.V. Chankin, D. Chiron, J. Christiansen, D. Ciric, S. Clement, J.P. Coad, I. Coffey<sup>7</sup>, S. Conroy<sup>15</sup>, G. Conway, S. Cooper, J.G. Cordey, G. Corrigan, G. Cottrell, S.J. Cox, R. Cusack, N. Davies, S.J. Davies, J.J. Davis, M. de Benedetti, H. de Esch, N. Deliyanakis, A. Dines, S.L. Dmitrenko, J. Dobbins, N. Dolgetta, S.E. Dorling, P.G. Doyle, H. Duquenoy, A.M. Edwards<sup>7</sup>, A.W. Edwards, J. Egedal, T. Elevant<sup>11</sup>, C.G. Elsmore, J. Ellis, S.K. Erents<sup>7</sup>, G. Ericsson<sup>15</sup>, L.G. Eriksson, H. Falter, J.W. Farthing, A. Fasoli<sup>3</sup>, M. Fichtmüller, G. Fishpool, K. Fullard, M. Gadeberg, L. Galbiati, R. Garbil, E. Gauthier<sup>20</sup>, A. Gibson, R.D. Gill, D. Godden, A. Gondhalekar, A. Goodyear, C. Gormezano, C. Gowers, F.S. Griph, M. Groth<sup>17</sup>, K. Guenther, H. Guo, A. Haigh, B. Haist<sup>4</sup>, C.J. Hancock, P.J. Harbour, J.D.W. Harling, N.C. Hawkes<sup>7</sup>, N.P. Hawkes<sup>1</sup>, R.F. Heeter<sup>13</sup>, J.L. Hemmerich, O.N. Hemming, T. Hender<sup>7</sup>, C.H.A. Hogben, L. Horton, M. Huart, G. Huysmans, C. Ingesson<sup>14</sup>, B. Ingram, M. Irving, J. Jacquinet, H. Jaeckel, J.F. Jaeger, O.N. Jarvis, M. Johnson, E.M. Jones, T.T.C. Jones, J-F. Junger, F. Junique, C. Jupen<sup>16</sup>, J. Kallne<sup>15</sup>, A. Kaye, B.E. Keen, M. Keilhacker, W. Kerner, N.G. Kidd, S. Knipe, J.G. Krom, P. Kupschus, R. LaHaye<sup>9</sup>, J.R. Last, K. Lawson<sup>7</sup>, M. Lennholm, J. Lingertat, X. Litaudon<sup>20</sup>, T. Loarer, P.J. Lomas, M. Loughlin, C. Lowry, R.M.A. Lucock, A.C. Maas<sup>14</sup>, B. Macklin, C.F. Maggi, M. Mantsinen<sup>5</sup>, V. Marchese, F. Marcus, J. Mart, D. Martin, G. Matthews, H. McBryan, G. McCracken, P.A. McCullen, A. Meigs, R. Middleton, P. Miele, F. Milani, J. Mills, R.D. Monk, P. Morgan, G. Murphy, F. Nave<sup>18</sup>, G. Newbert, P. Nielsen, P. Noll, W. Obert, D. O'Brien, M. O'Mullane, E. Oord, R. Ostrom, V.V. Parail, W. Parsons, B. Patel, A. Paynter, A. Perevezentsev, A. Peacock, R.J.H. Pearce, M.A. Pick, J. Plancoulaine, O. Pogutse, R. Prentice, S. Puppini, M. Rainford, V. Riccardo, F. Rimini, F. Rochard<sup>20</sup>, A. Rolfe, A.L. Roquemore<sup>13</sup>, R.T. Ross, G. Sadler, G. Saibene, R. Sartori, O. Sauter<sup>10</sup>, P. Schild, M. Schmid, V. Schmidt, B. Schunke, S. Sharapov, A. Sibley, M. Simon, R. Simonini, A.C.C. Sips, P. Smeulders, P. Smith, F. Söldner, J. Spence, R. Stagg, M. Stamp, P. Stangeby<sup>19</sup>, D.F.H. Start, D. Stork, P.E. Stott, J.D. Strachan<sup>13</sup>, B.C. Stratton<sup>13</sup>, P. Stubberfield, D. Summers, L. Svensson, P. Svensson, M. Tabellini, J. Tait, T. Tala<sup>6</sup>, A. Tanga, A. Taroni, C. Terella, D.S. Testa<sup>3</sup>, J.M. Todd, P.R. Thomas, K. Thomsen, E. Traneus<sup>15</sup>, B. Tubbing, P. Twyman, P. van Belle, G.C. Vlases, M. von Hellermann, T. Wade, R. Walton, D. Ward, M.L. Watkins, N. Watkins<sup>1</sup>, M.J. Watson, M.R. Wheatley, A. Whitehurst, D. Wilson, H.R. Wilson<sup>7</sup>, T. Winkel, D. Young, I.D. Young, K-D. Zastrow, W. Zwingmann.

### PERMANENT ADDRESSES

1. UKAEA, Harwell, Didcot, Oxon, UK.
2. University of Leicester, Leicester, UK.
3. Massachusetts Institute of Technology, USA.
4. KFA, Jülich, Germany.
5. Helsinki University of Technology, Espoo, Finland.
6. VTT Energy, Helsinki, Finland.
7. UKAEA Culham Laboratory, Abingdon, Oxon, UK.
8. A.F. Ioffe Institute, St. Petersburg, Russia.
9. General Atomics, San Diego, USA.
10. CRPP-EPFL, Lausanne, Switzerland.
11. Royal Institute of Technology, Stockholm, Sweden.
12. Imperial College, University of London, UK.
13. Princeton Plasma Physics Laboratory, Princeton, USA.
14. FOM Instituut voor Plasmafysica, Nieuwegein, The Netherlands.
15. Dept. of Neutron Research, Uppsala University, Sweden.
16. University of Lund, Sweden.
17. University of Manchester Institute of Science and Technology, Manchester, UK.
18. IST, Centro de Fúseo Nuclear, Lisbon, Portugal.
19. Institute for Aerospace Studies, University of Toronto, Canada.
20. CEA, Cadarache, France.

